Self-Consistent Stability Analysis of Ablation Fronts with Large Froude Numbers

In inertial-confinement fusion (ICF), the ablation front of the imploding capsules is hydrodynamically unstable.[1,2] The heavy material of the compressed pellet is accelerated by the low-density ablating plasma, thus making the pellet interface unstable to density perturbations (Rayleigh-Taylor instability).[3] The classical treatment[3] of this instability occurring at the interface of a heavy fluid with uniform density ρ_h, supported by a light fluid with uniform density ρ_l, yields the growth rate $\gamma_{cl} = \sqrt{A_T kg}$, where g is the acceleration and $A_T = (\rho_h - \rho_l)/(\rho_h + \rho_l)$ is the Atwood number. It is noteworthy that, in the classical case, the growth rate monotonically increases with the mode wave number k, and the Atwood number is constant. However, in ICF, the convection of ablated material through the interface leads to a reduction of the growth rate with respect to the classical value $(\gamma/\gamma_{cl} < 1)$ and, for sufficiently short wavelengths, the instability is suppressed.[4–20] Thus, only those modes with wave number smaller than a critical value[14–16] ($k < k_c$, where k_c is the cutoff wave number) are unstable. In addition, the density profile of ICF targets monotonically decreases in the ablation and blow-off regions, thus complicating the definition of a light-fluid density (ρ_l) to be used in the definition of the classical Atwood number. For a monotonic density profile and mode wavelength smaller than the density-gradient scale length,

$$kL >> 1, \quad \text{where} \quad L = \rho(d\rho/dy)^{-1},$$

the growth rate of the classical Rayleigh-Taylor instability (without ablative flow) is $\gamma_{cl} \simeq \sqrt{g/L_{\min}}$, where $L_{\min}$ is the minimum density-gradient scale length. This result has led several authors[1,20] to approximate the Atwood number with an asymptotic formula $(A_T = 1/1 + kL_{\min})$ that reproduces the classical results for long- and short-wavelength modes, and for $\rho_l << \rho_h$. In this article, the Atwood number is derived for equilibria with ablative flow, and it is shown that the classical formula does not apply to ablation fronts. The ablative Atwood number depends on the density-gradient scale length, the mode wavelength, and the law of thermal conduction.

A qualitative description of convective (or ablative) stabilization can be obtained by using the incompressible sharp boundary model[7–10] consisting of two fluids of constant density separated by an interface of zero thickness with mass flowing from the heavy to the light fluid. For subsonic ablation flows, the perturbed velocity field is assumed to be incompressible $(\nabla \cdot \tilde{\mathbf{v}} = 0)$ through the interface. It is easily shown that the assumption of divergence-free velocity perturbations is not consistent with an accelerating equilibrium flow, i.e., the equation describing the perturbation cannot be used to determine the equilibrium profiles. Since the equilibrium is one-dimensional, the incompressibility condition leads to a uniform velocity profile ($U = constant$), in clear contradiction with the mass conservation that requires a uniform mass flow ($\rho U = constant$) and a jump in the profiles. In addition, the model requires a closure equation, as the number of unknowns exceeds the number of equations. Several closure equations have been proposed by different authors[7–10] leading to discrepancies in the final results. In Ref. 10, the sharp boundary model is improved by a self-consistent calculation of the density jump occuring at the ablation front. Nevertheless, an additional closure equation [Eq. (5) of Ref. 9] is still needed and the model is not self-consistent.

Monotonic equilibrium profiles of ablation fronts can only be reproduced by retaining the effect of finite thermal conductivity in the energy equation. Thus, for consistency, the effect of thermal conduction should be retained in the stability analysis as well. Kull and Anisimov developed a model[4] (the isobaric model) that includes thermal conduction and neglects other less important physical effects such as finite Mach number. Their model is self-consistent because it can be solved to determine the equilibrium profiles as well as to carry out the stability analysis. However, in Ref. 4, Kull and Anisimov analytically solve the isobaric model without determining the self-consistent equilibrium. They assume instead that a sharp boundary exists between the heavy and the light fluids. Although their model is self-consistent, their solution is not. Later, Kull[5] numerically solves the self-consistent isobaric

model and finds a large discrepancy with the sharp boundary results. The numerical results of Kull[5] also agree with the results of Ref. 6. The latter can be fitted by the well-known formula

$$\gamma = \alpha_T \sqrt{kg} - \beta_T k V_a , \tag{1}$$

where V_a is the ablation velocity and α_T, β_T are given later in the section on **Stability Analysis**. This formula has been derived by numerically solving the exact eigenvalue problem, including electronic heat transport ($\kappa \sim T^{\nu}$, $\nu = 2.5$), for large Froude numbers (Fr = 5–9, see Table I of Ref. 5), where $Fr = V_a^2 / gL_0$ and L_0 is the characteristic width of the ablation front and will be specified in the next section. The numerical results of Kull[5] and Takabe[6] have also been confirmed by several two-dimensional simulations of accelerated targets and capsule implosions.[18,19]

The great difficulties in the analytic solution of the self-consistent problem had prevented the derivation of an analytic growth-rate formula that reproduces the numerical results. Only recently, some attempts have been made to close this gap by solving the self-consistent problem using asymptotic techniques.

The first attempt is found in Ref. 12, where the Wentzel-Kramers-Brillouin (WKB) approximation is used to determine the cutoff wave number in the case of electronic heat conduction ($\nu = 2.5$). Based on this analytic estimate, V. V. Bychkov, S. M. Goldberg, and M. A. Liberman derive an approximate growth-rate formula, similar to Eq. (1), with $\beta = 2.5$–3.2 and $\alpha^2 = (\rho_1 - \rho_2)/(\rho_1 + \rho_2)$, where ρ_1 is the peak density and ρ_2 is the critical density. In Ref. 16, the cutoff formula for long-wavelength modes and $Fr > 1$ is derived self-consistently for an arbitrary power law dependence of the thermal conduction $(\kappa \sim T^{\nu},\ \nu > 1)$ using boundary layer theory. The eigenvalue equation is solved in the overdense, ablation, and blowoff regions, and the solutions are asymptotically matched. For $\nu = 2.5$, this formula agrees with the analytic estimate of Ref. 12 and reproduces the numerical results of Ref. 5 for different values of ν.

A semi-analytical, self-consistent analysis is also carried out in Ref. 13 by matching the analytical solution of the ablation region with the numerical solution of the blowoff region. The growth rate of Ref. 13 and the fully analytic formula derived in this article are in agreement for $\nu = 2.5$ and $Fr > 10$, but significant discrepancies exist for large ν's. A more detailed comparison between analytical, semi-analytical, and numerical results is presented in the **Discussion** section.

In this article, the importance of a growth rate formula valid over a large range of ν's is emphasized. In fact, numerical simulations show that direct- and indirect-drive ICF capsule implosions have different instability growth rates. This could be related to the different mechanism of energy transport—indirect-drive ICF is dominated by radiation transport and direct drive by electronic thermal conduction. In the diffusive radiation model,[21] the heat flux transported by radiation heat conduction is proportional to the temperature gradient $(q = -\kappa \nabla T)$ and the effective radiation thermal conductivity $\kappa = 16\sigma T^3 l(T)/3$, where σ is the Stefan-Boltzmann constant, and $l(T)$ is the Rosseland mean free path. According to Ref. 21, $l(T)$ can be approximated by a power law with the power index dependent on the material properties. For example, in an optically thick, fully ionized homogeneous plasma, $l(T) \sim T^{3.5}$ and $\kappa \sim T^{6.5}$. The variance of the power index has provided the motivation to carry out the stability analysis for arbitrary values of ν ($\kappa \sim T^{\nu}$) and to determine a generalized formula for the growth rate.

In this article, we present the analytical solution of the eigenvalue problem derived from the linearized isobaric model of Kull and Anisimov[4] for long-wavelength perturbations ($kL << 1$), closing the gap between theory and numerical computations, and extending the validity of the growth-rate formula to a large range of ν's. The analysis is limited to $\nu > 1$ and large values of the Froude number, thus restricting the unstable spectrum to wavelengths longer than the width of the ablation front. In fact, as shown in Ref. 16, the cutoff wave number for large-Froude-number equilibria occurs at long wavelengths: $k_c L_0 \sim 1/Fr^{\frac{\nu}{\nu-1}} << 1$. Configurations with $Fr > 1$ are typical for ablation fronts characterized by pure electron heat conduction (such as those considered in Ref. 6), some indirectly driven targets with large ablation velocities, and some directly driven targets with a strong radiation emission [such as those containing poly-vinyl-chloride (PVC or C_2H_3Cl)].

The growth rate is obtained by performing a boundary layer analysis in the regions of different scale lengths for the perturbation and subsequent asymptotic matching. The analytic theory is compared with the numerical results of Kull[5] and Takabe[6] for different values of Fr and ν.

This article is organized as follows: First, the isobaric model describing the evolution of accelerated ablation fronts is presented; next, the equilibrium profiles are derived, a stability analysis is performed, and the growth-rate formulas are reported. Finally, in the discussion section, the growth-rate formulas are compared with the numerical results.

Isobaric Model

We consider an ablatively accelerated fluid in steady state. In the ablation-front frame of reference, the evolution of the mass density ρ, velocity $\mathbf{v}$, and temperature T is described by the following conservation equations:

$$\frac{\partial \rho}{\partial t} + \nabla \cdot \rho \mathbf{v} = 0 \tag{2}$$

$$\rho\left(\frac{\partial \mathbf{v}}{\partial t} + \mathbf{v} \cdot \nabla \mathbf{v}\right) = -\nabla p + \rho \mathbf{g} \tag{3}$$

$$\rho \mathbf{c}_v \left(\frac{\partial T}{\partial t} + \mathbf{v} \cdot \nabla T\right) = -p \nabla \cdot \mathbf{v} + \nabla \cdot \kappa \nabla T \ , \tag{4}$$

where $\mathbf{g} = g\mathbf{e}_\mathbf{y}(g<0)$, $p = \rho T/A$ is the hydrodynamic pressure, $c_v = A^{-1}/(\gamma_h - 1)$ is the specific heat at constant volume, and γ_h is the ratio of the specific heats. The constant $A = \rho/(n_i + n_e) \simeq m_i/(1+Z)$ represents the average particle mass, where m_i is the ion mass, Z is the atomic number, and n_i, n_e are the ion and electron particle densities, respectively. The thermal conductivity κ has a power law dependence on the temperature, $\kappa = \kappa_a (T/T_a)^\nu$, where T_a is the ablation temperature.

For realistic ICF implosions, the energy equation can be simplified by assuming that the sound speed C_s at the ablation surface is much larger than the ablation velocity V_a, i.e., a negligible Mach number M $(M = V_a/C_s << 1)$, and the density-gradient scale length $\left[L = \rho(d\rho/dy)^{-1}\right]$ is much smaller than the stratification length C_s^2/g. Following the work of Kull and Anisimov,[4] the simplified energy equation can be rewritten in divergence-free form,

$$\nabla \cdot \left(\mathbf{v} + L_0 V_a \frac{\nabla \xi}{\xi^{\nu+2}}\right) = 0, \tag{5}$$

where $\xi = \rho/\rho_a$ is the density normalized to its peak value ρ_a, and L_0 is the typical width of the ablation front,

$$L_0 \equiv \frac{\gamma_h - 1}{\gamma_h} \frac{A\kappa_a}{\rho_a V_a} \ . \tag{6}$$

For classical electron thermal conduction, $\nu = 5/2$, and κ_a is given by Spitzer,[22]

$$\kappa_a = \frac{32 T_a^{5/2}}{\pi^{3/2}\sqrt{2}\Phi(Z)\Lambda Z e^4 \sqrt{m_e}} \ , \tag{7}$$

where Λ is the Coulomb logarithm and

$$\Phi(Z) \simeq (Z + 4.16)/(Z + 0.24).$$

As will be shown later, the constant L_0 is proportional to the density-gradient scale length at the ablation front.

Equations (2), (3), and (5) represent a complete set of four equations for the four variables ρ, v_x, v_y, and p that can be used to study the equilibrium and stability of accelerated ablation fronts.

Equilibrium Profiles

The equilibrium profiles can be derived from Eqs. (2), (3), and (5) by setting $\partial/\partial t = 0$. Although a detailed description of such profiles is given by Kull in Ref. 5, we summarize herein the main results. The density profile obeys the following first-order differential equation obtained by combining Eqs. (2) and (5):

$$\frac{d\xi}{dy} = \frac{1}{L_0} \xi^{\nu+1}(\xi_0 - \xi), \tag{8}$$

where ξ_0 is an integration constant. The appropriate boundary conditions for ablation fronts require the density profile to be flat at the peak value ($\xi' = 0$ for $\xi = 1$, leading to $\xi_0 = 1$) and evanescent in the downstream or expansion region ($\xi \to 0$ for $y \to -\infty$). The steepness of the profile depends on the value of L_0 that is determined by the thermal conduction and the ablation rate. Using Eq. (8), the density-gradient scale length can be written as $L = L_0/\left[\xi^\nu(1-\xi)\right]$ and its minimum value[5] is proportional to L_0, $L_{\min} = \left[(\nu+1)^{\nu+1}/\nu^\nu\right] L_0$. As described in Ref. 16, the length L_0 can also be related to the distance L_e between the peak of the density and the 1/*e* point.

Although Eq. (8) cannot be solved in closed form, an approximate solution can be found in proximity of the peak

density (overdense region), where $y > 0$, $\xi \approx 1$, and in the blowoff region, where $y < 0$, $\xi << 1$:

$$\xi_{\text{overdense}} \approx 1 - e^{-y/L_0}, \quad \xi_{\text{blowoff}} \approx \left(-\frac{L_0}{\nu y}\right)^{1/\nu}. \quad (9)$$

Equation (9) shows that the density profile is sharp near the peak density, where $L \simeq L_0$, and becomes smooth in the expansion region, where $L \simeq -\nu y$ and $-y >> L_0$. The equilibrium velocity profile can easily be derived from the mass conservation equation $\left[\nabla \cdot (\rho \mathbf{U}) = 0\right]$. Since the ablated material is flowing toward the light fluid, then $\mathbf{U} = U\mathbf{e}_y$, $U < 0$, and $\rho U = const$. In the overdense region, the velocity U approaches a constant value $U(y \to \infty) = -V_a$, and its magnitude monotonically increases in the blowoff region $\left[U(y \to -\infty) \to -\infty\right]$.

It is important to observe that the density-, velocity-, and temperature-gradient scale lengths are determined by the thermal-conductivity coefficient, the ablation rate, and the power index ν. The profiles become smoother as κ_a or ν increases.

Stability Analysis

The linear stability analysis proceeds in the standard manner. Following Ref. 16, all perturbed quantities are written as $Q_1 = \tilde{Q}(y) \exp(ikx + \gamma t)$, and the linear equations can be combined into a single fifth-order differential equation,

$$\left[\partial_{\hat{y}}\left(\Gamma_a \xi + \partial_{\hat{y}}\right)\partial_{\hat{y}} - \left(\Gamma_a \xi + \partial_{\hat{y}}\right)\right]$$

$$\times \in \hat{L}\left[\left(\Gamma_a \xi + \partial_{\hat{y}}\right)\tilde{\Phi}\xi^{\nu} + \in \hat{\nabla}^2\tilde{\Phi}\right]$$

$$+ \partial_{\hat{y}}\left(\Gamma_a \xi + \partial_{\hat{y}}\right)\left[\partial_{\hat{y}}\tilde{\Phi}\xi^{\nu} + \in \hat{\nabla}^2\tilde{\Phi}\right]$$

$$+ \in \hat{\nabla}^2\tilde{\Phi} + \frac{1}{\in Fr}\tilde{\Phi}\xi^{\nu+2} = 0, \quad (10)$$

where $\tilde{\Phi} = \tilde{\rho}/\left(\rho\xi^{\nu+1}\right)$, $\hat{y} = ky$, $\Gamma_a = -\gamma/kV_a$, $Fr = V_a^2/|g|L_0$ is the Froude number, $\hat{\nabla} = k^{-1}\nabla$, $\in = kL_0$, and $\hat{L} = L/L_0$. Equation (10) is an eigenvalue equation for the growth rate $\gamma = -\Gamma_a kV_a$. The eigenfunction must satisfy the boundary conditions corresponding to a vanishing perturbation at infinity, i.e., $\tilde{\mathbf{v}}(\pm\infty) = 0$, $\tilde{p}(\pm\infty) = 0$, and $\tilde{\rho}(\pm\infty) = 0$. Because of the complicated spatial dependence of the coefficients, Eq. (10) cannot be solved in closed form. However, an approximated solution can be found for large values of Fr and long-wavelength modes ($Fr >> 1, \in << 1$). The presence of the small parameter $\in$ makes Eq. (10) solvable by asymptotic methods such as boundary layer theory. First, the equation is solved in regions of different scale lengths for the perturbations. Then, the solutions are asymptotically matched at the boundaries of each region. The asymptotic matching and the boundary conditions lead to a unique value of the growth rate γ. Using the shape of the density profile and the scale length of the perturbations, three regions can be identified (see Fig. 65.21): (1) the overdense region, where $\hat{y} >> \in$, (2) the ablation front, where $\hat{y} \sim \in$, and (3) the blowoff region, where $-\hat{y} >> \in$.

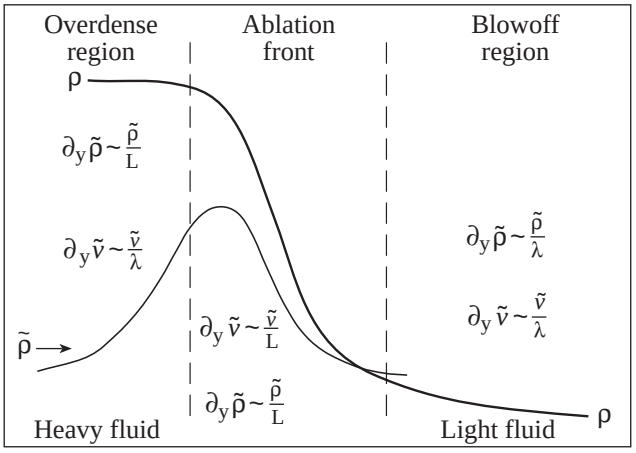

Figure 65.21
Density profile with regions of different scale lengths for the perturbations. Here λ is the mode wavelength.

Region 1: The Overdense Region

In ICF capsule implosions, the heavy-fluid region is the overdense portion of the shell where $\hat{y} \equiv ky \sim 1$, $\rho \simeq \rho_a$, $\xi \equiv \rho/\rho_a = 1 - \exp(-\hat{y}/\in) + O\left[\exp(-2\hat{y}/\in)\right]$, and $L >> L_0$. In this region and to lowest order in $\exp(-\hat{y}/\in)$, Eq. (10) reduces to a constant-coefficient fifth-order differential equation,

$$\left(\partial_{\hat{y}}^2 - 1\right)\left(\Gamma_a + \partial_{\hat{y}}\right)\left(\in \partial_{\hat{y}}^2 - \partial_{\hat{y}} + \Gamma_a - \in\right)\tilde{\Phi}^h \exp(\hat{y}/\in) = 0, \quad (11)$$

where $\Gamma_a = -\gamma/kV_a$ and the superscript h denotes the heavy-fluid region. The solution of Eq. (11) can be written in the following form:

$$\tilde{\Phi}^h = \left(a^h e^{-\hat{y}} + b^h e^{\alpha^- \hat{y}} + c^h e^{\hat{y}} + d^h e^{-\Gamma_a \hat{y}} + q^h e^{\alpha^+ \hat{y}}\right) e^{-\hat{y}/\epsilon}, \quad (12)$$

where a^h, b^h, c^h, d^h, q^h are integration constants and $\alpha^{\pm} = \left[1 \pm \sqrt{1 + 4\epsilon(\epsilon - \Gamma_a)}\right] / 2\epsilon$. In order to satisfy the boundary conditions of vanishing perturbations at $+\infty$, $c^h = d^h = q^h = 0$, and Eq. (12) reduces to the simple form

$$\tilde{\Phi}^h = \left(a^h e^{-\hat{y}} + b^h e^{\alpha^- \hat{y}}\right) e^{-\hat{y}/\epsilon}. \quad (13)$$

It is important to observe that the incompressible theory $(\nabla \cdot \tilde{\mathbf{v}} = 0)$ yields only the sonic solution

$$\tilde{\rho}_{\text{sonic}} \sim \exp\left[-\hat{y} - \hat{y}/\epsilon\right].$$

Equation (13) shows that a new solution is introduced by the finite thermal conductivity and, because of its diffusive character, we denote the second term in Eq. (13) as the diffusion or entropy solution. The asymptotic matching conditions can be greatly simplified by the following choice of the integration constants:

$$a^h = 1 - b^h, \qquad b^h = B^h - \hat{\beta}\frac{\epsilon^{1/\nu}}{\Gamma_a}, \quad (14)$$

where B^h, $\hat{\beta}$ must be determined from asymptotic matching, and the normalization condition $a^h + b^h = 1$ has been used. The heavy-fluid solution [Eq. (13)] can be rewritten using the ablation-front variable $z = \hat{y}/\epsilon$ and expanding α^- in powers of ϵ and $\epsilon\Gamma_a$,

$$\alpha^- \simeq \Gamma_a\left[1 - \frac{\epsilon^2}{\epsilon\Gamma_a} + \epsilon\Gamma_a - 2\epsilon^2 + 2(\epsilon\Gamma_a)^2 + \ldots\right]. \quad (15)$$

A short calculation yields

$$\tilde{\Phi}^h(\hat{y} \sim \epsilon) = e^{-z}\left[\Psi^h(\epsilon z) + \tilde{\chi}^h(\epsilon\Gamma_a, \epsilon, z)\right], \quad (16)$$

where $\Psi^h(\epsilon z)$ and $\tilde{\chi}^h(\epsilon\Gamma_a, \epsilon, z)$ can be written as an ϵ-series

$$\Psi^h(\epsilon z) = 1 - \epsilon z\left[1 - b^h(1 - \epsilon) + \hat{\beta}\epsilon^{1/\nu}\right] + \left(1 - b^h\right)\left[\epsilon^2\frac{z^2}{2} - \epsilon^3\frac{z^3}{6} + O(\epsilon^4)\right], \quad (17a)$$

$$\tilde{\chi}^h(\epsilon\Gamma_a, \epsilon, z) = \sum_{j=0}^{\infty} \tilde{\chi}_j(\epsilon\Gamma_a, z)\epsilon^j. \quad (17b)$$

It is important to observe that the parameter $\epsilon\Gamma_a$ is small for long-wavelength modes and large Froude numbers. Indeed, $\epsilon|\Gamma_a| = \epsilon\gamma/(kV_a) < \epsilon\gamma_{cl}/(kV_a) = \sqrt{\epsilon/Fr} \ll 1$. Thus, each term of the series in Eq. (17b) can be further expanded in powers of $\epsilon\Gamma_a$:

$$\tilde{\chi}_0^h = B^h(\epsilon\Gamma_a)z + b^h\left[(\epsilon\Gamma_a)^2\left(z + \frac{z^2}{2}\right) + (\epsilon\Gamma_a)^3\left(\frac{z^3}{6} + z^2 + 2z\right)\right] + b^h\left\{(\epsilon\Gamma_a)^4\left(\frac{z^4}{24} + \frac{z^3}{2} + \frac{5}{2}z^2 + 5z\right) + O\left[(\epsilon\Gamma_a)^5\right]\right\}, \quad (18a)$$

$$\tilde{\chi}_1^h = 0, \ \tilde{\chi}_2^h = -2b^h\left\{(\epsilon\Gamma_a)\left(z + \frac{z^2}{2}\right) + O\left[(\epsilon\Gamma_a)^2\right]\right\}. \quad (18b)$$

The next step is to solve Eq. (10) in the ablation-front region and asymptotically match that solution with Eq. (16).

Region 2: The Ablation-Front Region

The ablation front is the region where the density, velocity, and temperature profiles undergo sharp variations. In this region, $\hat{y} \sim \epsilon$, $L \sim L_0$, and $\xi \sim 1$. Since $\xi \equiv \rho/\rho_a \sim 1$, Eq. (8) cannot be analytically solved and an explicit expression for the spatial dependence of the density profile cannot be found. Thus, it is more convenient to use ξ as the independent variable in Eq. (10). By denoting $\tilde{\Phi}^a$ as the solution in the ablation region and after some straightforward manipulations, Eq. (10) can be rewritten in the following operator form:

$$\left[L_0 + \epsilon L_1 + \epsilon^2 L_2 + \epsilon^4 L_4\right]\tilde{\Phi}^a = 0, \quad (19)$$

where

$$L_0 = \partial_z(\in\Gamma + \partial_z)\partial_z\left[\in\Gamma\hat{L}\xi^\nu + \left(\hat{L}\partial_z + 1\right)\left(\xi^\nu + \partial_z\right)\right], \quad (20a)$$

$$L_1 = \frac{\xi^{\nu+2}}{\Gamma_c^2}\left(\in\Gamma_a\right)^2, \quad (20b)$$

$$L_2 = -\partial_z(\in\Gamma + \partial_z)\partial_z\hat{L} - (\in\Gamma + \partial_z)\hat{L}\left[(\in\Gamma + \partial_z)\xi^\nu + \partial_z^2\right] - \partial_z \in\Gamma, \quad (20c)$$

$$L_4 = \in\Gamma\hat{L} + \partial_z\hat{L} - 1, \quad (20d)$$

$\partial_z = \xi^{\nu+1}(1-\xi)\partial_\xi$, $\hat{L} = \xi^{-\nu}/(1-\xi)$, $\Gamma = \Gamma_a\xi$, $\Gamma_c \equiv \gamma\sqrt{k|g|}$, and $z = \hat{y}/\in$ is the ablation-front coordinate ($z \sim 1$ in the ablation-front region). Furthermore, each operator L_i can be expanded in powers of $\in\Gamma_a$, and the eigenfunction can be expressed as a double power series,

$$L_i = \sum_{j=0}^{\infty} L_{ij}\left(\in\Gamma_a\right)^j,$$
$$\tilde{\Phi}^a = \sum_{j=0}^{\infty} \tilde{\Phi}_j^a \in^j, \quad (21)$$
$$\tilde{\Phi}_j^a = \sum_{k=0}^{\infty} \tilde{\Phi}_{jk}^a\left(\in\Gamma_a\right)^k.$$

The next step is to solve Eq. (19) order by order. To lowest order in $\in$ and $\in\Gamma_a$, Eq. (19) yields

$$\tilde{\Phi}_{00}^a = A^a\Psi_0 + B^a\Psi_1 + C^a\Psi_2 + D^a\Psi_3 + E^a\Psi_4, \quad (22)$$

where A^a, B^a, C^a, D^a, and E^a are the integration constants. The five solutions can be written in the following integral forms:

$$\Psi_0 = \frac{1-\xi}{\xi}, \qquad \Psi_1 = \frac{1-\xi}{\xi}z(\xi), \quad (23a)$$

$$\Psi_2 = \frac{1-\xi}{\xi}\left\{\frac{z^2(\xi)}{2} + \frac{1}{\nu}\int_1^\xi \frac{T_\nu(\eta)}{\eta^{\nu+1}(1-\eta)^2}\,d\eta\right\}, \quad (23b)$$

$$\Psi_3 = \frac{1-\xi}{\xi}\left\{\frac{z^3(\xi)}{6} - \int_1^\xi \frac{d\eta}{\eta^{\nu+1}(1-\eta)^2}\int_1^\eta z(x)\frac{1-x^{\nu+1}}{x^{\nu+1}}dx\right\}, \quad (23c)$$

$$\Psi_4 = \frac{1-\xi}{\xi}\int_{\xi(0)}^\xi \frac{d\eta}{\eta^{\nu+1}(1-\eta)^2}, \quad (23d)$$

$$z(\xi) = \int_{\xi(0)}^\xi \frac{d\eta}{\eta^{\nu+1}(1-\eta)}, \quad (23e)$$

where $T_\alpha(x) = 1/x^\alpha + \alpha(x-1) - 1$, and $\xi(0)$ is the density at $z = 0$. To determine the integration constants, the solution in the ablation front must be asymptotically matched with the solution in the heavy-fluid region. This can be accomplished by taking the limit of $\xi \to 1 (z \to \infty)$ in Eq. (22). According to standard boundary layer theory, the asymptotic matching will occur if a common region of validity of the two solutions exists. Substituting $1-\xi = e^{-z} + O\left(e^{-2z}\right)$ and matching the lowest-order term of Eq. (22) with Eq. (16) yields $B^a = C^a = D^a = E^a = 0$, and $A^a = 1$. The first- and second-order matchings in $\in\Gamma_a$ yield $\tilde{\Phi}_{01}^a = B^h\Psi_1$, $\tilde{\Phi}_{02}^a = b^h\left(\Psi_1 + \Psi_2\right)$. The functions $\tilde{\Phi}_{03}^a$ and $\tilde{\Phi}_{04}^a$ can also be derived from Eq. (19) and, because of the lengthy expressions, they are reported in Appendix A.

The next step is to solve Eq. (19) to zeroth order in $\in\Gamma_a$ and first/second order in $\in$, i.e.,

$$L_{00}\tilde{\Phi}_{10}^a = 0 \quad \text{and} \quad L_{00}\tilde{\Phi}_{20}^a = -L_{20}\tilde{\Phi}_{00}^a.$$

Matching the $\in$ and $\in^2$ terms of the solutions with Eq. (16) yields

$$\tilde{\Phi}_{10}^a = -B_1^a\Psi_1, \quad \tilde{\Phi}_{20}^a = \frac{1-\xi}{\xi}\frac{z^2}{2} - b^h\Psi_2, \quad (24)$$

where $B_1^a = 1 - b^h(1-\in) + \hat{\beta}\in^{1/\nu}$. The functions $\tilde{\Phi}_{12}^a$ and $\tilde{\Phi}_{21}^a$ are important to describe the eigenfunction $\tilde{\Phi}^a$ to the desired accuracy; they are also reported in Appendix A.

Region 3: The Blowoff Region

The blowoff or expansion region is located downstream with respect to the ablation front. In this region, $-\hat{y} \sim 1$, $L >> L_0$, and $\xi \simeq \left(-L_0/\nu y\right)^{1/\nu} << 1$. The analysis can be simplified by introducing the new variable

$$\varsigma = \epsilon \Big/ \left(\nu \xi^{\nu}\right) = -\hat{y}\left[1 + O(\xi)\right],$$

and rewriting Eq. (10) in the following form:

$$\frac{1}{\nu} M_0 \tilde{\Phi}^l + \sigma M_1 \tilde{\Phi}^l + \sigma^2 M_2 \tilde{\Phi}^l = 0, \tag{25}$$

where $\sigma = \left[\left|\Gamma_a\right|^{\nu} (\epsilon/\nu)\right]^{-1/\nu}$, and the superscript *l* denotes variables in the low-density fluid,

$$M_0 = \left[\left(\partial_{\hat{y}} \frac{1}{\varsigma^{1/\nu}} \partial_{\hat{y}} - \frac{1}{\varsigma^{1/\nu}}\right) \frac{1}{1-\xi} + \frac{1}{\nu \epsilon Fr \Gamma_a^2} \frac{1}{\zeta^{\frac{\nu+1}{\nu}}}\right] \frac{1}{\zeta^{1/\nu}}, \tag{26a}$$

$$\begin{aligned} M_1 = {} & -\partial_{\hat{y}} \hat{\nabla}^2 \frac{1}{\nu \zeta^{1/\nu}(1-\xi)} \\ & - \left[\partial_{\hat{y}} \frac{1}{\zeta^{1/\nu}} + \left(\partial_{\hat{y}} \frac{1}{\zeta^{1/\nu}} \partial_{\hat{y}} - \frac{1}{\zeta^{1/\nu}}\right) \frac{\zeta}{1-\xi}\right] \\ & \times \left(\partial_{\hat{y}} \frac{1}{\nu\zeta} + \hat{\nabla}^2\right), \end{aligned} \tag{26b}$$

$$M_2 = \frac{1}{\nu}\left(\partial_{\hat{y}}^4 + \partial_{\hat{y}}^3 \frac{1}{\nu\zeta} - 1\right) + \partial_{\hat{y}} \hat{\nabla}^2 \frac{\zeta}{1-\xi}\left(\partial_{\hat{y}} \frac{1}{\nu\zeta} + \hat{\nabla}^2\right), \tag{26c}$$

$\partial_{\hat{y}} = -(1-\xi)\partial_{\zeta}$, and $\xi = (\epsilon/\nu\zeta)^{1/\nu}$. Focusing on the values of $\nu > 1$, Eq. (25) yields different solutions according to the magnitude of $\sigma\nu$: (1) $\sigma\nu << 1$ and (2) $\sigma\nu >> 1$.

Solution 1: $\sigma\nu << 1$

Since the growth rate of the long-wavelength modes ($\epsilon << 1$) scales as the classical growth rate $\left(\gamma \sim \sqrt{kg}\right)$, the condition $\sigma\nu << 1$ can be rewritten in the following form:

$$\epsilon^{\frac{\nu-2}{\nu}} \nu^{\frac{2\nu+2}{\nu}} Fr << 1. \tag{27}$$

For large Froude numbers, Eq. (27) can be satisfied only for density profiles with $\nu > 2$ and wave numbers

$$\epsilon << \left(\frac{1}{\nu^{\frac{2\nu+2}{\nu}} Fr}\right)^{\frac{\nu}{\nu-2}}. \tag{28}$$

Since σ and $\epsilon^{1/\nu}$ are small, the differential operator and the eigenfunction can be expanded in powers of σ and $\epsilon^{1/\nu}$,

$$\begin{aligned} M_j &= \sum_{k=0}^{\infty} M_{jk} \epsilon^{k/\nu}, \\ \tilde{\Phi}^l &= \sum_{n=0}^{\infty} \tilde{\Phi}_n^l \sigma^n, \quad \tilde{\Phi}_n^l = \sum_{i=0}^{\infty} \tilde{\Phi}_{ni}^l \epsilon^{i/\nu}. \end{aligned} \tag{29}$$

Each term of the series satisfies the boundary condition $\tilde{\Phi}_{ni}^l(\zeta \to \infty) = 0$. Substituting Eq. (29) into Eq. (25) and collecting terms corresponding to the lowest power of σ and $\epsilon^{1/\nu}$ leads to $M_{00}\tilde{\Phi}_{00}^l = 0$, which results in

$$\left[\zeta \partial_{\zeta}^2 - \frac{1}{\nu}\partial_{\zeta} - \zeta + \frac{1}{\nu \epsilon Fr \Gamma_a^2}\right] \tilde{\Phi}_{00}^l \zeta^{-1/\nu} = 0. \tag{30}$$

The solution of Eq. (30) satisfying the boundary conditions at infinity can be written in terms of the Kummers' confluent hypergeometric function $U(a, b, x)$,

$$\begin{aligned} \tilde{\Phi}_{00}^l &= C_l \zeta^{1/\nu} e^{-\zeta} U(a, b, 2\zeta), \\ a &= -\frac{1}{2\nu \epsilon Fr \Gamma_a^2} - \frac{1}{2\nu}, \quad b = -\frac{1}{\nu}. \end{aligned} \tag{31}$$

The other terms of the series in Eq. (29) can be found from Eq. (25) in a similar manner. Particularly useful for matching is the term $\tilde{\Phi}_{10}^l$ that satisfies $M_{00}\tilde{\Phi}_{10}^l / \nu = -M_{10}\tilde{\Phi}_{00}^l$. However, because of its complexity, we simplify such an equation by assuming that, to lowest order in ϵ, $\epsilon^{1/\nu}$, and $\epsilon\Gamma_a$, the eigenvalue has the classical form $\gamma^2 = k|g|$. This assumption is verified later by the matching conditions. First, observe that for $\gamma^2 = k|g|$, Eq. (31) reduces to

$$\tilde{\Phi}_{00}^l = C_l \zeta^{1/\nu} e^{\zeta} \Gamma(1 + 1/\nu, 2\zeta),$$

where $\mathbf{\Gamma}(a, x)$ is the incomplete gamma function. By rewriting $M_{10} = -\hat{\nabla}^2 \zeta \hat{\nabla}^2 \zeta^{-1/\nu}$ and substituting $\tilde{\Phi}_{00}^l$ into Eq. (25), the equation for $\tilde{\Phi}_{10}^l$ can be solved in closed form, yielding

$$\tilde{\Phi}_{10}^l = \frac{2^{1/\mu} C_l}{\nu} e^{\zeta} \zeta^{1/\nu} \left[\Gamma(2/\nu, 2\zeta) - \nu\Gamma(1 + 2/\nu, 2\zeta)\right], \tag{32}$$

where $\mu = \nu/(\nu - 1)$. To achieve matching with the solution in

the ablation front, it is important to derive the asymptotic behavior of the solution in the blowoff region for small ζ. Combining Eqs. (31) and (32) leads to the following form of the eigenfunction:

$$\tilde{\Phi}^l_{00} + \sigma\tilde{\Phi}^l_{10} = C_l\zeta^{1/\nu}\left\{A_l\left(1+a_l\zeta+\ldots\right) - B_l\left(2\zeta\right)^{1+\frac{1}{\nu}}\left(1+b_l\zeta+\ldots\right) - 2^{1/\nu}\sigma\,\zeta^{2/\nu}\left(1+\zeta+\ldots\right)\right\}, \tag{33}$$

where

$$A_l = \frac{\Gamma\left[1+1/\nu\right]}{\Gamma\left[1+a+1/\nu\right]} - \frac{2^{1/\mu}\sigma}{\nu}\Gamma\left[\frac{2}{\nu}\right], \tag{34a}$$

$$a_l = \frac{1}{A_l}\left\{\frac{\Gamma\left[1+1/\nu\right]}{\Gamma\left[1+a+1/\nu\right]}\left(2\frac{a}{b}-1\right) - \frac{2^{1/\mu}\sigma}{\nu}\right\}, \tag{34b}$$

$$B_l = \frac{\nu}{\nu+1}\frac{\Gamma\left(-1/\nu\right)}{\Gamma\left[a\right]}, \qquad b_l = 2\frac{1+a}{b} - 3. \tag{34c}$$

Substituting $\zeta = \epsilon\big/\left(\nu\xi^{\nu}\right)$, Eq. (33) can be rewritten as the sum of three power series in ϵ. It is important to observe that the power series in Eq. (33) cannot be matched with the ϵ and $\epsilon\,\Gamma_a$ power series of the ablation-front solution. This suggests that a transition region exists between the ablation front and the blowoff regions. The solution in such a region must match the ablation front as well as the blowoff region solution.

By introducing the layer variable $\eta = \zeta/\sigma^{\mu}$ and the operator $\partial_u = -\left(1-\xi\right)\partial_{\eta}$, Eq. (25) can be rewritten in the following form:

$$W_0\tilde{\Phi}^t + \Delta W_1\tilde{\Phi}^t + \Delta^2 W_2\tilde{\Phi}^t + \Delta^4 W_4\tilde{\Phi}^t = 0, \tag{35}$$

where $\Delta = \sigma^{\mu}$, the superscript t denotes the transition region, and

$$W_0 = \partial_u\left(\partial_u - \frac{1}{\eta^{1/\nu}}\right) \times \partial_u\left\{\frac{\eta}{1-\xi}\left[\left(\partial_u - \frac{1}{\eta^{1/\nu}}\right)\frac{1}{\nu\eta} + \partial_u^2\right] + \frac{1}{\nu}\partial_u + \frac{1}{\nu^2\eta}\right\}, \tag{36a}$$

$$W_1 = \frac{1}{\nu^2\,\epsilon\,Fr\Gamma_a^2}\,\frac{1}{\eta^{\frac{\nu+2}{\nu}}}, \tag{36b}$$

$$W_2 = \frac{1}{\nu}\partial_u\frac{1}{\eta^{1/\nu}} - \left(\partial_u - \frac{1}{\eta^{1/\nu}}\right)\frac{\eta}{1-\xi}\left[\partial_u^2 + \left(\partial_u - \frac{1}{\eta^{1/\nu}}\right)\frac{1}{\nu\eta}\right] - \partial_u\left(\partial_u - \frac{1}{\eta^{1/\nu}}\right)\partial_u\frac{\eta}{1-\xi}, \tag{36c}$$

$$W_4 = \left(\partial_u - \frac{1}{\eta^{1/\nu}}\right)\frac{\eta}{1-\xi} - \frac{1}{\nu}, \tag{36d}$$

and $\xi = \left(\epsilon/\Delta\nu\eta\right)^{1/\nu}$. Observe that $\epsilon/\Delta \sim \left(\epsilon/Fr\right)^{\frac{\nu}{2(\nu-1)}} << 1$, and the variable $\xi \sim \left(\epsilon/\Delta\right)^{1/\nu} << 1$. Thus, each operator W_i can be expanded in powers of $\left(\epsilon/\Delta\right)^{1/\nu}$, and the eigenfunction $\tilde{\Phi}^t$ can be expanded in powers of Δ and $\left(\epsilon/\Delta\right)^{1/\nu}$,

$$W_i = \sum_{n=0}^{\infty} W_{in}\left(\frac{\epsilon}{\Delta}\right)^{n/\nu}, \qquad \tilde{\Phi}^t = \sum_{n=0}^{\infty}\tilde{\Phi}^t_n\Delta^n, \quad \tilde{\Phi}^t_n = \sum_{j=0}^{\infty}\tilde{\Phi}^t_{nj}\left(\frac{\epsilon}{\Delta}\right)^{j/\nu}. \tag{37}$$

To lowest order in Δ and $\left(\epsilon/\Delta\right)^{1/\nu}$, Eq. (35) reduces to $W_{00}\tilde{\Phi}^t_{00} = 0$, where

$$W_{00} = -\frac{1}{\nu^2}\partial_{\eta}\left(\partial_{\eta} + \frac{1}{\eta^{1/\nu}}\right) \times \partial_{\eta}\left(\nu^2\eta\partial_{\eta}^2 - 2\nu\partial_{\eta} + \frac{\nu+1}{\eta} - \frac{\nu}{\eta^{1/\nu}}\right). \tag{38}$$

This equation can be further simplified by introducing a new function $\tilde{\chi}^t = \tilde{\Phi}^t/\eta^{1/\nu}$ and by integrating three times with respect to η. A straightforward manipulation leads to the following second-order differential equation:

$$\nu\eta^{2-\frac{1}{\mu}}\partial_{\eta}^2\tilde{\chi}^t - \tilde{\chi}^t = A^t\int_0^{\eta}d\theta\; e^{-\mu\theta^{1/\mu}}\int_0^{\theta}d\phi\; e^{\mu\phi^{1/\mu}} + B^t\int_0^{\eta}d\theta\; e^{-\mu\theta^{1/\mu}} - C^t, \tag{39}$$

where A^t, B^t, C^t are the constants of integration. The solution of Eq. (39) can be written as a linear combination of the

homogeneous and particular solutions,

$$\tilde{\chi}^t = A^t\chi_A^P + B^t\chi_B^P + C^t\chi_C^P + D^t\chi_D^H + E^t\chi_E^H, \quad (40)$$

where $\chi_A^P, \chi_B^P, \chi_C^P$ are the particular solutions corresponding to each term in the right-hand side of Eq. (39) and χ_D^H, χ_E^H are the homogeneous solutions (D^t and E^t are integration constants). Next, we observe that $\chi_C^P = 1$ and we rewrite Eq. (39) for the other four solutions by introducing the new variable $\tau = \eta^{1/\mu}$. A short calculation yields

$$\nu\tau\partial_\tau^2\tilde{\chi}^t - \mu\partial_\tau\tilde{\chi}^t - \mu^2\tilde{\chi}^t = \mu^2\Pi(\tau), \quad (41a)$$

where

$$\Pi(\tau) = A^t\mu^2\int_0^\tau d\theta\left(\theta^{\mu/\nu}e^{-\mu\theta}\right)\int_0^\theta d\phi\left(\phi^{\mu/\nu}e^{\mu\phi}\right) + B^t\mu\int_0^\tau d\theta\left(\theta^{\mu/\nu}e^{-\mu\theta}\right). \quad (41b)$$

The homogeneous solutions can be easily calculated from Eq. (41a), yielding

$$\chi_D^H = \tau^{\mu/2}\,\mathbf{K}_\mu\left(2\mu\sqrt{\tau/\nu}\right), \qquad \chi_E^H = \tau^{\mu/2}\,\mathbf{I}_\mu\left(2\mu\sqrt{\tau/\nu}\right), \quad (42)$$

where $\mathbf{K}_\mu(x)$ and $\mathbf{I}_\mu(x)$ are the modified Bessel functions. To determine the two particular solutions χ_A^P and χ_B^P, Eq. (41a) is transformed in Laplace space,

$$\frac{d\hat{\chi}^t}{ds} + \left[\frac{2\nu+\mu}{\nu s} + \frac{\mu^2}{\nu s^2}\right]\hat{\chi}^t = A^tF_A(s) + B^tF_B(s). \quad (43)$$

The Laplace transforms of χ_A^P and χ_B^P are the particular solutions of Eq. (43):

$$\hat{\chi}_A^P = -\frac{\mu^4}{\nu}\Gamma(2\mu)\frac{e^{\mu^2/\nu s}}{s^{2+\frac{\mu}{\nu}}}\int_{1/s}^\infty\frac{e^{-\frac{\mu^2 x}{\nu}}}{(1+x\mu)^\mu}dx\int_0^x dy\left(y+\mu y^2\right)^{\mu/\nu}, \quad (44)$$

$$\hat{\chi}_B^P = -\mu\left(\frac{\mu}{\nu}\right)^\mu\frac{\Gamma(\mu)}{s^{2+\frac{\mu}{\nu}}}e^{\frac{\mu}{\nu}\left(1+\frac{\mu}{s}\right)}\Gamma\left[1-\mu,\frac{\mu}{\nu}\left(1+\frac{\mu}{s}\right)\right], \quad (45)$$

where

$$F_A(s) = -\frac{\mu^4}{\nu s^3}\frac{\Gamma(2\mu)}{(s+\mu)^\mu}\int_s^\infty\frac{(\omega+\mu)^{\mu/\nu}}{\omega^{2\mu}}d\omega, \qquad F_B(s) = -\frac{\mu^3}{\nu s^3}\frac{\Gamma(\mu)}{(s+\mu)^\mu}. \quad (46)$$

Here, $\mathbf{\Gamma}(x)$ is the gamma function and $\mu = \frac{\nu}{\nu-1}$. The behavior of the particular solutions for $\tau\to\infty$ and $\tau\to 0$ can be determined by expanding Eqs. (44) and (45) in proximity of the poles. A short calculation yields

$$\chi_A^P(\tau\approx 0) = \phi_1\tau^\mu\left[1+\frac{\mu}{2\nu-1}\tau+\cdots\right] + \phi_2\tau^{2\mu+1}\left[1-\frac{\nu}{2(3\nu-2)}\tau+\cdots\right], \quad (47a)$$

$$\chi_A^P(\tau\to\infty) = -\frac{\nu}{\nu+1}\tau^{2\mu-1}\left[1+\frac{\nu+1}{2\nu\tau}+\cdots\right], \quad (47b)$$

$$\chi_B^P(\tau\approx 0) = \theta_1\tau^\mu\left[1+\frac{\mu}{2\nu-1}\tau\cdots\right] + \theta_2\tau^{\mu+1}\left[1-\frac{\nu}{2(3\nu-2)}\tau\cdots\right], \quad (47c)$$

$$\chi_B^P(\tau\to\infty) = -\Gamma(\mu)\mu^{-\mu/\nu} - \frac{1}{\mu\nu}\tau^{\mu-2}e^{-\mu\tau}, \quad (47d)$$

where

$$\phi_1 = -\frac{\Gamma(2\mu)}{\nu-1}\Gamma\left(\frac{\nu+1}{1-\nu},\frac{\mu}{\nu}\right)\left(\frac{\in}{\nu}\right)^{\mu/\nu}, \qquad \phi_2 = \frac{\nu}{2(3\nu-1)(2\nu-1)}, \quad (48a)$$

$$\theta_1 = -\left(\frac{\mu}{\nu}\right)^\mu e^{\mu/\nu}\,\Gamma\left(-\frac{\mu}{\nu},\frac{\mu}{\nu}\right), \qquad \theta_2 = \frac{\nu}{(\nu-1)(2\nu-1)}. \quad (48b)$$

Equations (47) and (48) determine the lowest-order solution in the transition region. By inspection, one can immediately

conclude that the exponentially growing solution χ_E^H does not match the solution in the light-fluid region, and the χ_D^H generates an $\in\Gamma_a$ series for $\eta = \in/\nu\Delta\xi^\nu$ that cannot be matched by the ablation layer solution. Thus, we set $D^t = E^t = 0$ in Eq. (40) and rewrite the transition region solution as

$$\tilde{\Phi}_{00}^t = C^t\tilde{\Phi}_{00}^C + A^t\tilde{\Phi}_{00}^A + B^t\tilde{\Phi}_{00}^B,$$

where

$$\tilde{\Phi}_{00}^C = \eta^{1/\nu},\quad \tilde{\Phi}_{00}^A = \eta^{1/\nu}\chi_A^P,\ \text{and}\ \tilde{\Phi}_{00}^B = \eta^{1/\nu}\chi_B^P.$$

Some higher-order terms in the Δ and $\xi \sim (\in/\Delta)^{1/\nu}$ series are also important; they are reported in Appendix B.

The growth rate of the instability can be found by matching the solutions in the ablation front, the transition, and the blowoff region. First, we combine the terms of the transition region into a single function

$$\tilde{\Phi}^t = C^t\left(\tilde{\Phi}_0^C + \Delta\tilde{\Phi}_1^C + \Delta^2\tilde{\Phi}_{20}^C + \cdots\right) + A^t\left[\tilde{\Phi}_{00}^A + \Delta\tilde{\Phi}_{10}^A + \left(\frac{\in}{\nu\Delta}\right)^{1/\nu}\tilde{\Phi}_{01}^A + \cdots\right] + B^t\eta^{1/\nu}\chi_B^P. \quad (49)$$

Then, we rewrite the transition region solution near the ablation region by substituting $\eta = \in/\nu\,\Delta\xi^\nu$ into Eq. (49) and taking the limit of $\xi \to 0$,

$$\begin{aligned}\tilde{\Phi}^t(\eta\to 0,\xi\to 0) &= C^t\left(\frac{\in}{\Delta\nu}\right)^{1/\nu}\\ &\times\frac{1}{\xi}\left(1-\frac{\in}{\xi^\nu}\frac{kg}{\nu\gamma^2}+\frac{\in^2}{2\nu^2\xi^{2\nu}}+\cdots\right)\\ &+\left\{A^t\phi_1\left[1+O(\Delta,\xi)\right]+B^t\theta_1\right\}\left(\frac{\in}{\nu\Delta}\right)^{\frac{\nu+1}{\nu}}\frac{F_1(\xi)}{\xi^{\nu+1}}\\ &+A^t\phi_2\left(\frac{\in}{\Delta\nu}\right)^3\frac{F_2(\xi)}{\xi^{3\nu}}(1+Q_3\xi+\cdots)\\ &+B^t\left(\frac{\in}{\Delta\nu}\right)^2\frac{\theta_2}{\xi^{2\nu}}F_2(\xi). \end{aligned} \quad (50)$$

Equation (50) must match the ablation-front solution in the limit of $\xi \to 0$. The asymptotic behavior of the ablation-front solution near $\xi = 0$ can be obtained from the section covering the **Ablation-Front Region**, leading to

$$\begin{aligned}\tilde{\Phi}^a &\to \frac{R_0}{\xi}+\in\frac{R_1}{\xi^{\nu+1}}+\in^2\frac{1}{2\nu^2\xi^{2\nu+1}}\\ &-\in\Gamma_a\frac{B^h+\in\Gamma_a b^hQ_1}{\nu\xi^{\nu+1}}F_1(\xi)-\in^{2+\frac{1}{\nu}}\Gamma_a\frac{\hat{\beta}Q_2}{\xi^{2\nu}}\\ &\times\left(1+\frac{\in\Gamma_a}{\nu}\right)F_2(\xi)\\ &-\in^3\Gamma_a^2\left\{B_1^a+\frac{kg}{\gamma^2}-\hat{\beta}\in^{1/\nu}F_2(\xi)\left[1+Q_3\xi+\cdots\right]\right\}\frac{Q_4}{\xi^{3\nu}}, \end{aligned} \quad (51)$$

where

$$\begin{aligned}R_0 &= 1-\in z_0\left(1-b^h\right)+\in\Gamma_aB^hz_0,\\ R_1 &= \frac{1}{\nu}\left[B_1^a-\in z_0\left(1-b^h\right)-\in b^h\frac{\nu+1}{\nu}\right],\end{aligned} \quad (52a)$$

$$Q_1 = \frac{\nu z_0-1}{\nu},\quad Q_2 = \left[\nu(2\nu-1)(\nu-1)\right]^{-1}, \quad (52b)$$

$$\begin{aligned}Q_3 &= \frac{9\nu^3-11\nu^2+4\nu}{(\nu-1)^2(3\nu-2)},\\ Q_4 &= \left[2\nu^2(2\nu-1)(3\nu-1)\right]^{-1},\end{aligned} \quad (52c)$$

$$F_1(\xi) = 1-\frac{\in\Gamma_a}{(2\nu-1)(\nu-1)\xi^{\nu-1}} + \frac{(\in\Gamma_a)^2}{2(\nu-1)^2(2\nu-1)(3\nu-2)\xi^{2(\nu-1)}}+\cdots, \quad (52d)$$

$$F_2(\xi) = 1+\frac{\in\Gamma_a}{2(3\nu-2)\xi^{\nu-1}}+\cdots. \quad (52e)$$

Here, $z_0 = \sum_{n=0}^{\infty}\xi(0)^{n-\nu}/(\nu-n)$. Matching Eq. (50) with Eq. (51) yields the following set of equations:

$$R_0 = C^t\left(\frac{\in}{\nu\Delta}\right)^{1/\nu},\qquad -\frac{kg}{\gamma^2} = \frac{\nu R_1}{R_0}, \quad (53a)$$

$$B^h = -\left(\frac{\in}{\nu\Delta}\right)^{1/\nu}\frac{A^t\phi_1\left[1+O(\Delta,\xi)\right]+B^t\theta_1}{\Delta\Gamma_a\left(1+\in\Gamma_aQ_1/B^h\right)}, \quad (53b)$$

$$B^t = \nu^{1/\nu}\Delta^{\frac{\nu+1}{\nu}}\hat{\beta}\left(1+\frac{\in\Gamma_a}{\nu}\right), \tag{53c}$$

$$-\frac{kg}{\gamma^2} = 1 - b^h(1-\in) + \frac{A^t}{\Delta^3\Gamma_a^2}. \tag{53d}$$

The next step is to match the solutions for the transition and blowoff regions. Taking the limit of Eq. (48) for $\eta \to \infty$ and $\Delta \to 0$ yields

$$\tilde{\Phi}^t(\eta\to\infty,\Delta\to 0) = \left[C^t - \Gamma(\mu)\mu^{\frac{1}{1-\nu}}B^t - \phi_1 A^t\left(\frac{\in}{\nu\Delta}\right)^{1/\nu}\right]\eta^{1/\nu}\left[1+O(\Delta\eta)\right] - A^t\frac{\nu}{\nu+1}\left(1+\frac{kg}{\gamma^2}\phi_1\right)\eta^{1+\frac{2}{\nu}}\left[1+O(\Delta\eta)\right]. \tag{54}$$

Upon the substitution $\zeta = \Delta\eta$, the terms of this equation must match the powers of η in Eq. (33). A short calculation yields

$$A^t\left(\frac{\in}{\nu\Delta}\right)^{1/\nu} = \sum^l \Delta^{\frac{\nu+1}{\nu}}R_0, \qquad \sum^l = 2^{\frac{\nu+1}{\nu}}\frac{\nu+1}{\nu}\frac{B^l}{A^l}\frac{1+O\left(\in^{1/\nu}\Delta\right)}{1+\frac{kg}{\gamma^2}\phi_1\Delta}. \tag{55}$$

Equations (53) and (55) determine the order of magnitude of the constants. It is easy to show that $B^h \sim \Delta^{1/\nu}/\Gamma_a << 1$, $B^t \sim \Delta^{(\nu+1)/\nu} \sim A^t\xi << A^t$, and $\hat{\beta} \sim 1$. Equations (53) and (55) can be used to determine the instability growth rate and the parameter $\hat{\beta}$. Retaining all terms up to order $\in\Gamma_a B^h$ and $\in$, the instability growth rate satisfies the following equation:

$$\gamma(k << k_c) = \sqrt{A_T\, k|g|} - \beta k V_a, \tag{56}$$

where

$$A_T = \frac{1-\mu_0\in^{1/\nu}}{1+\mu_0\in^{1/\nu}}, \quad \mu_0 = \frac{(2/\nu)^{1/\nu}}{\Gamma\left(\frac{\nu+1}{\nu}\right)}, \quad \beta = \frac{\Gamma\left(\frac{\nu+2}{\nu}\right)}{\Gamma^2\left(\frac{\nu+1}{\nu}\right)}. \tag{57}$$

Equation (56) represents the growth rate of the instability for $\nu > 2$ and

$$k L_0 << \left[\nu^{(2\nu+2)/\nu}Fr\right]^{\nu/(2-\nu)}.$$

Solution 2: $\sigma\nu >> 1$

For $\sigma\nu >> 1$, the solution of Eq. (25) can be determined by following the procedure described in Ref. 16. The differential operators and the eigenfunction are expanded in powers of $1/\nu$:

$$M_i = \sum_{n=0}^{\infty} M_{in}\left(\frac{1}{\nu}\right)^n, \qquad \tilde{\Phi}^l = \sum_{n=0}^{\infty}\tilde{\Phi}_n^l(\hat{y})\left(\frac{1}{\nu}\right)^n, \tag{58}$$

where i = 0,1,2. Substituting Eq. (58) into Eq. (25) and collecting terms up to the first two orders in $1/\nu$ yields the following equations:

$$\left(\Gamma_a\delta + \partial_{\hat{y}}\right)\left(\partial_{\hat{y}}^2 - 1\right)\varsigma\left(\partial_{\hat{y}}^2 - 1\right)\tilde{\Phi}_0^l = 0, \tag{59}$$

$$\left(\Gamma_a\delta + \partial_{\hat{y}}\right)\left(\partial_{\hat{y}}^2 - 1\right)\varsigma\left(\partial_{\hat{y}}^2 - 1\right)\tilde{\Phi}_1^l + \left(\Gamma_a\delta + \partial_{\hat{y}}\right)\left(\partial_{\hat{y}}^2 - 1\right)\varsigma\partial_{\hat{y}}\frac{\tilde{\Phi}_0^l}{\varsigma} + \left\{\Gamma_a\delta\left(\Gamma_a\delta + \partial_{\hat{y}}\right) - \frac{\delta}{1-\delta}\left(\Gamma_a\delta + \partial_{\hat{y}}\right)\left(\partial_{\hat{y}}^2 - 1\right)\varsigma\ln\varsigma - \Gamma_a\delta\left(\partial_{\hat{y}}\ln\varsigma\partial_{\hat{y}} - \ln\varsigma\right)\varsigma + (1-\delta)\left[\partial_{\hat{y}}\left(\Gamma_a\delta + \alpha_{\hat{y}}\right) + 1\right]\right\} \times \left(\partial_{\hat{y}}^2 - 1\right)\tilde{\Phi}_0^l = 0, \tag{60}$$

where

$$\delta = (\in/\nu)^{1/\nu}, \quad \varsigma = \in\Big/\left(\nu\xi^\nu\right), \text{ and } \partial_{\hat{y}} = -(1-\xi)\partial_\varsigma.$$

The function $\tilde{\Phi}_0^l$ can be written as a combination of the three decaying homogeneous solutions of Eq. (59):

$$\tilde{\Phi}_0^l = A^l\tilde{\Phi}_A^l + B^l\tilde{\Phi}_B^l + C^l\tilde{\Phi}_C^l,$$

where

$$\tilde{\Phi}_A^l = e^{\hat{y}}, \quad \tilde{\Phi}_B^l = e^{-\hat{y}}\int_{-\infty}^{\hat{y}} dx e^{2x}\int^x \frac{d\eta}{\varsigma(\eta)}, \tag{61a}$$

$$\tilde{\Phi}_C^l = e^{\hat{y}} \int_0^{\hat{y}} dx e^{-2x} \int_{-\infty}^{x} d\eta \frac{e^{2\eta} - e^{\eta(1-\Gamma_a\delta)}}{\varsigma(\eta)}. \quad (61b)$$

The next step is to determine the coefficients A^l, B^l, C^l by matching the solution $\tilde{\Phi}_0^l$ with the ablation-front solution $\tilde{\Phi}^a$. Using the $1/\nu$ expansion of the ablation-front solution,

$$\begin{aligned}\tilde{\Phi}^a = {} & \frac{1-\delta}{\delta} + \frac{1}{\nu}\frac{\ln\varsigma}{\delta} + \frac{\varsigma}{\delta}\left[1 - b^h\left(1+\Gamma_a\right)\right] \\ & \times\left[1 + \frac{1}{\nu}\left(\ln\varsigma + \frac{\delta}{1-\delta}\right)\right] \\ & + \frac{\varsigma^2}{2(1-\delta)^2}\left\{\frac{1-\delta}{\delta} + \frac{1}{\nu}\left[2 - b^h\left(1-\Gamma_a^2\right) + \left(\frac{1}{\delta} - 2\right)\ln\varsigma\right]\right\} \\ & + \frac{\varsigma^3}{6\delta(1-\delta)^2}\left\{1 - b^h\left(1+\Gamma_a\right) + \frac{1}{2\nu}\left[\left(1 - b^h\left[1+\Gamma_a\right]\right)\right.\right. \\ & \times\frac{1+5\delta+2\ln\varsigma(1-3\delta)}{(1-\delta)} \\ & \left.\left. + \frac{\delta}{\in Fr} - \Gamma_a\delta\left[\Gamma_a - b^h\left(1+\Gamma_a\right)\right]\right\} + O\left(\frac{1}{\nu^2}\right),\end{aligned} \quad (62)$$

and matching the lowest power of $1/\nu$ in $\tilde{\Phi}^a$ and $\tilde{\Phi}_0^l$ yields $A^l = (1-\delta)/\delta$, $B^l = C^l = 0$.

The first-order correction $\tilde{\Phi}_1^l$ can be obtained by solving Eq. (60),

$$\tilde{\Phi}_1^l = \frac{\ln\varsigma}{\delta} e^{\hat{y}} + (1-\delta) C_1^l \tilde{\Phi}_C^l. \quad (63)$$

The constants C_1^l, b^h, and the dispersion relation are determined by matching $\tilde{\Phi}_0^l$ and $\tilde{\Phi}_1^l$ with Eq. (62):

$$\begin{aligned} b^h &= \frac{2}{1+\Gamma_a}\left[1 - \frac{\delta}{\nu(1-\delta)}\ln\left(\frac{2}{1-\delta\Gamma_a}\right)\frac{1-\Gamma_a}{1+\delta\Gamma_a}\right], \\ C_1^l &= 2\frac{1-\Gamma_a}{1+\delta\Gamma_a}, \end{aligned} \quad (64)$$

$$\Gamma_a^2 - \frac{4}{1+\delta}\Gamma_a - \left(\frac{1-\delta}{\in Fr(1+\delta)} - \frac{1}{\delta}\right) = 0. \quad (65)$$

Solving Eq. (65) yields the growth-rate formula:

$$\gamma = \sqrt{A_T^0 k|g| - \left(A_T^0\right)^2 k^2 V_a V_{bo}^0} - \left(1 + A_T^0\right) kV_a, \quad (66)$$

where

$$A_T^0 = \frac{1 - (\in/\nu)^{1/\nu}}{1 + (\in/\nu)^{1/\nu}}, \qquad V_{bo}^0 = \frac{V_a}{(\in/\nu)^{1/\nu}}. \quad (67)$$

Note the different coefficients of $\in^{1/\nu}$ in the Atwood numbers defined by Eqs. (67) and (57). It is important to remember that Eq. (66) has been derived using the $1/\nu$ expansion and, to the lowest order in $1/\nu$, $\mu_0 = (1/\nu)^{1/\nu}$ and $A_T^0 = A_T$. Furthermore, replacing A_T^0 with A_T and V_{bo}^0 with $V_a/\left(\mu_0 \in^{1/\nu}\right)$ in Eq. (66) would also reproduce the cutoff wave number obtained in Ref. 16 by including the higher-order corrections in $1/\nu$. Thus, we conclude that replacing $(\in/\nu)^{1/\nu}$ with $\mu_0 \in^{1/\nu}$ in Eq. (66) improves the accuracy of the growth-rate formula up to the first order in $1/\nu$:

$$\gamma = \sqrt{A_T k|g| - A_T^2 k^2 V_a V_{bo}} - \left(1 + A_T\right) kV_a, \quad (68)$$

where

$$V_{bo} = \frac{V_a}{\mu_0 \in^{1/\nu}}, \quad A_T = \frac{1 - \mu_0 \in^{1/\nu}}{1 + \mu_0 \in^{1/\nu}}. \quad (69)$$

Although Eq. (68) is valid over a large range of ν's > 1, a significant degradation of its accuracy is expected to occur for $\nu \to 1$, where the $1/\nu$ expansion breaks down. This problem is addressed in the next section, where the range of validity of the growth-rate formulas is discussed.

Summary of the Growth-Rate Formulas for *Fr* >> 1

For values of $\nu > 2$, two different growth-rate formulas have been derived according to the magnitude of the wave number:

$$\gamma = \sqrt{A_T k|g|} - \beta kV_a, \text{ for } kL_0 << \left(\nu^{2+\frac{2}{\nu}} Fr\right)^{\frac{\nu}{2-\nu}}, \quad (70a)$$

and

$$\gamma = \sqrt{A_T k|g| - A_T^2 k^2 V_a V_{bo}} - \left(1 + A_T\right) kV_a, \text{ for } kL_0 >> \left(\nu^{2+\frac{2}{\nu}} Fr\right)^{\frac{\nu}{2-\nu}}, \quad (70b)$$

where A_T, β, and V_{bo} are defined by Eqs. (57) and (69), respectively.

For values of $1 < \nu < 2$, the analysis of the previous section still applies. However, because corrections due to higher orders of $1/\nu$ are not included in the derivation, the growth-rate formula [Eq. (68)] shows poor agreement with the numerical results for $\nu < 1.5$. Figure 65.22(a) shows the unstable spectrum obtained by Eq. (68) and the numerical results of Ref. 5 for $\nu = 1.5$, 1.2, and 1.15. Note the degradation in accuracy of the analytic growth rate for $\nu < 1.5$. The analytic formula can be improved by observing that, for $\nu \to 1$, the cutoff wave number is so small that the $\in^{1/\nu}$ corrections can be neglected in the analysis and the eignevalue equation can be numerically solved in the blowoff region. It is found that by modifying μ_0 to $\mu_0 + 0.12/\nu^2$, the matching conditions are satisfied over a large range of Froude numbers and $\nu \to 1^+$, thus leading to a general growth-rate formula valid for $1 < \nu < 2$:

$$\gamma = \sqrt{A_T k|g| - A_T^2 k^2 V_a V'_{bo}} - (1 + A_T) kV_a, \qquad (71a)$$

where

$$V'_{bo} = \frac{V_a}{\mu'_0 \in^{1/\nu}}, \qquad \mu'_0 = \mu_0 + \frac{0.12}{\nu^2}, \qquad (71b)$$

and A_T is defined by Eq. (57). Figure 65.22(b) shows that for values of ν close to unity, excellent agreement is obtained between the numerical results of Ref. 5 and the modified formula [Eq. (71)].

Discussion

The validity of the asymptotic formula has been tested by comparing the growth rate obtained from Eqs. (70) and (71) with the numerical results of Ref. 5, where the isobaric model is numerically solved. Figure 65.23 shows plots of the normalized growth rate $\gamma L_0/V_a$ calculated using Eq. (70) (solid lines) and one numerically derived in Ref. 5 for $\nu = 2.5$ for different values of the Froude number (dots). Remarkable agreement between numerical and analytical results is obtained. In Fig. 65.24, the analytic growth rate is compared with the numerical results of Ref. 5 for different values of ν and fixed Froude number. The solid lines represent the result of the analytic theory and the dots are the numerical results. The analytic formula [Eq. (70)] is also compared with the self-consistent growth rate derived in Ref. 13. A significant disagreement between the results of Ref. 13 and Eq. (70) is found for large values of ν. Figure 65.25 shows the plot of the unstable spectrum for $\nu = 8$ obtained from the numerical computations of Kull[4] (dashed line), Eq. (70) (solid line), and the growth-rate formula of Ref. 13 with zero Mach number (dotted line).

Next, Eq. (70) is compared with other growth-rate formulas obtained by fitting numerical results. The most commonly used formula has been derived by Takabe *et al*. in Ref. 6 for spherical geometry, electronic heat conduction ($\nu = 2.5$), and large values of the Froude number. Following Ref. 6, the numerically derived growth rate can be fitted by the following formula:

$$\gamma = \alpha_T \sqrt{kg} - \beta_T kV_a, \qquad (72)$$

where

$$\alpha_T = 0.9\, G^{-0.02},$$

$$\beta_T = 2.3\left(\frac{\rho_a}{\rho_s}\right)^{0.075} G^{-0.2}, \qquad (73)$$

$$G = gr_s/c_s^2,$$

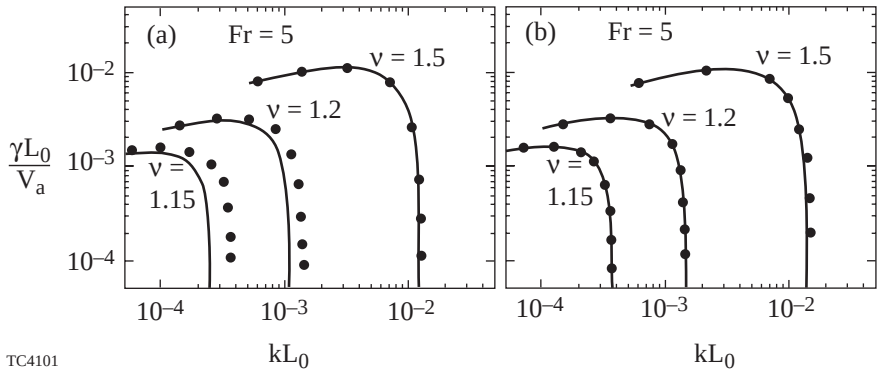

Figure 65.22
Unstable spectrum ($\gamma L_0/V_a$ versus kL_0) calculated using (a) Eq. (68) and (b) Eq. (71) (solid lines) compared with the numerical results of Ref. 5 (dots) for $\nu = 1.5$, 1.2, and 1.15 and $Fr = 5$.

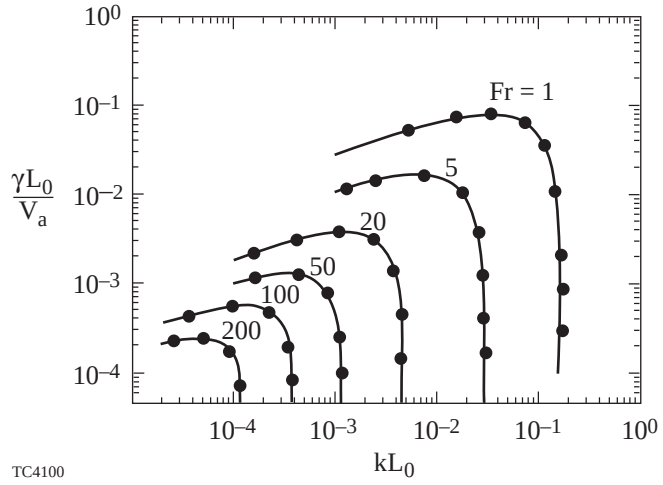

Figure 65.23
Unstable spectrum ($\gamma L_0/V_a$ versus kL_0) calculated using Eq. (70) (solid lines) compared with the numerical results of Ref. 5 (dots) for $\nu = 2.5$.

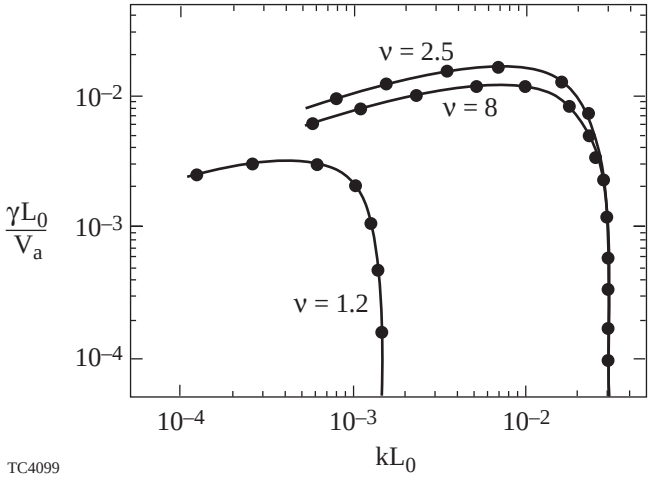

Figure 65.24
Unstable spectrum ($\gamma L_0/V_a$ versus kL_0) calculated using Eqs. (70) and (71) (solid lines) compared with the numerical results of Ref. 5 (dots) for $\nu = 1.2$, 2.5, 8 and $Fr = 5$.

and ρ_s, c_s, and r_s are the sonic density, sound speed, and position of the sonic point, respectively. Since α_T is almost independent of the equilibrium parameters ($\alpha_T \simeq 0.9$), we focus our attention on β_T. It is important to remember that, while Eqs. (72) and (73) have been derived for spherical geometry including finite Mach number, Eq. (70) is valid for slab geometry, neglecting the Mach number. Since the only isobaric dimensionless parameter is the Froude number, the coefficient β_T must be rewritten in terms of Fr. Using the isobaric profiles [Eq. (9)], we define y_s as the distance at which $\xi(y_s) = \rho_s/\rho_a \simeq (L_0/\nu y_s)^{1/\nu} << 1$, and correlate the parameter G to the Froude number,

$$G = \frac{0.4}{Fr}\,\frac{r_s}{y_s}\left(\frac{r_s}{r_a}\right)^4\left(\frac{\rho_a}{\rho_s}\right)^{0.5}, \qquad (74)$$

where r_a is the radial location of the peak density. Table I of Ref. 5 shows values of the relevant dimensionless parameters for $G = 2$. According to these values, Takabe's coefficients can be rewritten in the following form:

$$\beta_T = 1.8\,\theta\, Fr^{0.2},$$
$$\theta = \left(\frac{10\,y_s}{3\,r_s}\right)^{0.2}\left(\frac{10\,r_a}{9\,r_s}\right)^{0.8}\left(\frac{50\,\rho_s}{\rho_a}\right)^{0.025}. \qquad (75)$$

Observe that θ is very weakly dependent on the equilibrium parameters, and its values are always close to unity $(\theta \simeq 1)$. Table 65.I shows the values of θ corresponding to the equili-

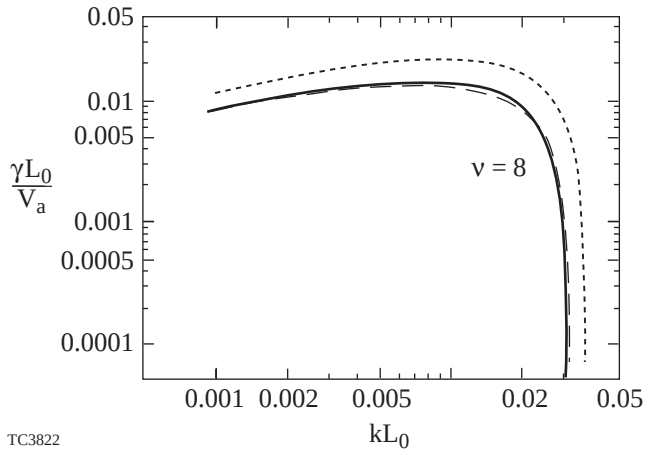

Figure 65.25
Plot of the normalized growth rate versus $\in$ for $\nu = 8$ and $Fr = 5$. The solid line represents Eq. (70), the dashed line is the numerical result of Ref. 5, and the dotted line is Eq. (16) of Ref. 13.

Table 65.I: Equilibrium parameters of Refs. 5 and 6.

$G = 2$				
r_a/r_s	Fr	ρ_a/ρ_s	y_s/r_s	θ
0.899	5.88	25.0	0.26	0.99
0.903	7.14	50.0	0.30	1.00
0.904	8.70	98.0	0.34	1.01

bria in Table I of Ref. 5. Since θ is approximately constant, the coefficient β depends mainly on the Froude number. The next step is to find the best fit ($\gamma_{\rm fit}$) for Eq. (70) based on a formula similar to Takabe's $\left(\gamma_{\rm fit} = a\sqrt{kg} - bkV_a\right)$. The fitting procedure is straightforward. The error $\left(\gamma - \gamma_{\rm fit}\right)^2$ is minimized over the portion of the unstable spectrum of interest to ICF ($1\ \mu{\rm m} < \lambda < 200\ \mu{\rm m}$). Since the typical cutoff wavelength λ_c is of the order of $1\ \mu$m, the minimization condition can be written in the convenient form

$$\frac{\partial \varepsilon}{\partial a} = 0, \qquad \frac{\partial \varepsilon}{\partial b} = 0, \quad \varepsilon = \int_{\lambda_c}^{200\lambda_c} \left(\gamma - \gamma_{\rm fit}\right)^2 d\lambda . \quad (76)$$

The two minimizing conditions yield the values of a and b that are subsequently fit with a power law formula ($a \sim Fr^{\mu_a}$ and $b \sim Fr^{\mu_b}$). For the values of Fr reported in Table I of Ref. 5 ($5 < Fr < 9$), the described procedure leads to the following fit of Eq. (70):

$$\gamma_{\rm fit} = 0.9\, Fr^{0.03}\sqrt{kg} - 2.0\, Fr^{0.15}\, kV_a . \quad (77)$$

The good agreement between Eqs. (77) and (72) confirms the accuracy of the analytic derivation. Furthermore, the general analytic formulas [Eqs. (70) and (71)] are valid for any $\nu > 1$ and can be applied to configurations that are not described by pure electron heat conduction.

Conclusions

The stability analysis of accelerated ablation fronts is carried out self-consistently for an arbitrary power law dependence of the thermal conductivity ($\kappa \sim T^{\nu}$ with $\nu > 1$) and large Froude numbers ($Fr > 1$). The eigenvalue equation is solved in different regions of the density profile (overdense, ablation, and blow-off regions), and the solution is asymptotically matched. The growth-rate formula is derived from the matching conditions, and its validity has been tested against the numerical results of Ref. 5. The excellent agreement between the growth-rate formula and the numerical results shows the high level of accuracy of the analytic derivation.

ACKNOWLEDGMENT

This work was supported by the U.S. Department of Energy Office of Inertial Confinement Fusion under Cooperative Agreement No. DE-FC03-92SF19460, the University of Rochester, and the New York State Energy Research and Development Authority. The support of DOE does not constitute an endorsement by DOE of the views expressed in this article.

Appendix A: Higher-Order Correction to $\tilde{\Phi}$ in the Ablation-Front Region

In this appendix, important higher-order corrections to the eigenfunction in the ablation-front region are reported. Those corrections are terms of Eq. (21), and they are derived by solving Eq. (19) order by order. After a very lengthy calculation, these terms can be written in the following convenient form:

$$\tilde{\Phi}^a_{03} = \frac{1-\xi}{\xi}\left\{ b^h\left[\frac{z^3}{6} + z^2 + 2z - \int_1^{\xi} \frac{G_{03}(\eta)}{\eta^{\nu+1}(1-\eta)^2}\, d\eta\right] - \frac{\hat{\beta}\,\epsilon^{1/\nu}}{\Gamma_a} K_{03}(\xi)\right\}, \quad (A1)$$

$$\tilde{\Phi}^a_{04} = \frac{1-\xi}{\xi}\left\{ b^h\left[\frac{z^4}{24} + \frac{z^3}{2} + \frac{5z^2}{2} + 5z\right] - \int_1^{\xi} \frac{d\eta}{\eta^{\nu+1}(1-\eta)^2} \int_1^{\eta} dx \left(b^h G_{04} - \frac{\hat{\beta}\,\epsilon^{1/\nu}}{\nu\Gamma_a} K_{04}\right)\right\}, \quad (A2)$$

$$\tilde{\Phi}^a_{11} = 0, \qquad \tilde{\Phi}^a_{21} = \tilde{\Phi}^{par}_{21} - 2b^h\left(\Psi_1 + \Psi_2\right), \quad (A3)$$

$$\tilde{\Phi}^{par}_{21} = \frac{1-\xi}{\xi}\int_1^{\xi} \frac{d\eta}{\eta^{\nu+1}(1-\eta)^2} \int_1^{\eta} dx \left\{ \frac{b^h}{\nu}\int_1^x \frac{T_{\nu-1}(y)}{y^{\nu+1}(1-y)^2}\, dy + B^h G_{21}(x)\right\}, \quad (A4)$$

$$\tilde{\Phi}^a_{12} = \left[B^a_1 + \frac{kg}{\gamma^2}\right]\frac{1-\xi}{\nu\xi}\int_1^{\xi} \frac{d\eta}{\eta^{\nu+1}(1-\eta)^2} \int_1^{\eta} dx \int_1^x \frac{1-y^{\nu}}{y^{2\nu+1}(1-y)}\, dy, \quad (A5)$$

where $T_a(x)$ is derived in the section on the **Ablation-Front Region** and

$$G_{03}(\eta)=\int_1^\eta dx\left[\left(\frac{1}{x^{\nu+1}}-1\right)(z+2)+\right.$$

$$\left.\frac{1}{\nu}\int_1^x \frac{T_\nu(y)}{y^{\nu+1}(1-y)^2}dy\right], \quad \text{(A6)}$$

$$K_{03}(\xi)=\frac{1}{\nu}\int_1^\xi \frac{d\eta}{\eta^{\nu+1}(1-\eta)^2}$$

$$\int_1^\eta dx\int_1^x \frac{1-y^\nu}{y^{2\nu+1}(1-y)}dy, \quad \text{(A7)}$$

$$G_{04}(x)=\left(\frac{1}{x^{\nu+1}}-1\right)\left(\frac{z^2}{2}+3z+5\right)$$

$$-\int_1^x \frac{dy}{y^{\nu+1}(1-y)^2}G_{03}(y), \quad \text{(A8)}$$

$$K_{04}(x)=\int_1^x \frac{dy}{y^{\nu+1}(1-y)}$$

$$\left[\int_1^y \frac{ds}{s^{2\nu}}\frac{1-s^\nu}{1-s}+\frac{1}{1-y}\int_1^y ds\int_1^s \frac{1-r^\nu}{r^{2\nu+1}(1-r)}dr\right], \quad \text{(A9)}$$

$$G_{21}(x)=-\frac{1}{\nu+1}\int_1^x \frac{y^{\nu+1}-1}{y^{2\nu+2}(1-y)}dy+z\left(\frac{1}{x^{\nu+1}}-1\right). \quad \text{(A10)}$$

Note that these corrections are essential to the derivation of Eqs. (51) and (62).

Appendix B: Higher-Order Correction to $\tilde{\Phi}$ in the Transition Region

In this appendix, the higher-order corrections to the eigenfunction in the transition region are reported. Those corrections are terms of Eq. (37), and they are derived by solving Eq. (35) order by order. The ξ and Δ corrections to $\tilde{\Phi}_{00}^C$ and $\tilde{\Phi}_{00}^A$ can be written in the following form:

$$\tilde{\Phi}_0^C=\eta^{1/\nu}(1-\xi), \quad \text{(B1)}$$

$$\tilde{\Phi}_1^C=-\frac{kg}{\gamma^2}\eta^{1/\nu}(1-\xi)\int_0^\eta \frac{d\eta}{1-\xi}, \quad \text{(B2)}$$

$$\tilde{\Phi}_2^C=\frac{1}{2}\eta^{2+\frac{1}{\nu}}\left[1+\frac{\nu+1}{\nu-1}\xi+O(\xi^2)\right]+O\left(1-\frac{kg}{\gamma^2}\right), \quad \text{(B3)}$$

$$\tilde{\Phi}_{10}^A=\frac{kg}{\gamma^2}\eta^{1/\nu}\chi_E^H(\eta)\int_\infty^\eta \frac{dx}{\left[\chi_E^H(x)\right]^2}$$

$$\int_0^x \frac{H_{10}(y)\chi_E^H(y)}{\nu y^{1+\frac{1}{\nu}}}dy+\frac{kg}{\gamma^2}\phi_1\tilde{\Phi}_{00}^A(\eta), \quad \text{(B4)}$$

$$\tilde{\Phi}_{01}^A=\eta^{1/\nu}\chi_E^H(\eta)\int_\infty^\eta \frac{dx}{\left[\chi_E^H(x)\right]^2}\int_0^x \frac{H_{01}(y)\chi_E^H(y)}{\nu y^{1+\frac{1}{\nu}}}dy$$

$$+\phi_1\eta^{1/\nu}\left[\frac{2}{\Gamma(\mu)}\left(\frac{\mu}{\sqrt{\nu}}\right)^\mu \chi_D^H(\eta)-1\right], \quad \text{(B5)}$$

where χ_E^H, χ_D^H, and $\tilde{\Phi}_{00}^A$ are defined in **Solution 2: $\sigma\nu$ >> 1,** and

$$H_{10}(y)=-\int_0^y drH_{00}(r)+\int_0^y d\theta e^{-\mu\theta^{1/\mu}}$$

$$\int_0^\theta d\phi\left[\phi-\partial_\phi\chi_A^P(\phi)\right]e^{\mu\phi^{1/\mu}}, \quad \text{(B6)}$$

$$H_{00}(r)=\int_0^r d\theta e^{-\mu\theta^{1/\mu}}\int_0^\theta d\phi e^{\mu\phi^{1/\mu}}, \quad \text{(B7)}$$

$$H_{01}(\eta)=\left(\frac{2}{\eta^{1/\nu}}-\frac{\nu+1}{\nu\eta}\right)\chi_A^P(\eta)$$

$$+\frac{H_{00}(\eta)}{\eta^{1/\nu}}-\frac{2}{\nu-2}\eta+\frac{1}{\nu-2}K_{01}(\eta), \quad \text{(B8)}$$

$$K_{01} = \int_0^{\eta} d\theta e^{-\mu\theta^{1/\mu}}$$

$$+\left(\nu\eta^{\frac{\nu-1}{\nu}}+1\right)e^{-\mu\eta^{1/\mu}}\int_0^{\eta} d\phi e^{\mu\phi^{1/\mu}} . \qquad \text{(B9)}$$

Observe that Eqs. (B1) and (B2) include all the ξ-corrections to $\tilde{\Phi}_{00}^{C}$ and $\tilde{\Phi}_{10}^{C}$. These terms are essential for the derivation of Eqs. (49) and (50).

REFERENCES

1. J. D. Kilkenny, S. G. Glendinning, S. W. Haan, B. A. Hammel, J. D. Lindl, D. Munro, B. A. Remington, S. V. Weber, J. P. Knauer, and C. P. Verdon, Phys. Plasmas **1**, 1379 (1994).
2. J. Grun *et al*., Phys. Rev. Lett. **58**, 2672 (1987); M. Desselberger *et al*., *ibid*. **65**, 2997 (1990); S. G. Glendinning, S. V. Weber, P. Bell, L. B. DaSilva, S. N. Dixit, M. A. Henesian, D. R. Kania, J. D. Kilkenny, H. T. Powell, R. J. Wallace, P. J. Wegner, J. P. Knauer, and C. P. Verdon, *ibid*. **69**, 1201 (1992); B. A. Remington *et al*., Phys. Fluids B **5**, 2589 (1993).
3. G. Taylor, Proc. R. Soc. London Ser. A **201**, 192 (1950); Lord Rayleigh, *Scientific Papers* (Cambridge University Press, Cambridge, England, 1900), Vol. II, pp. 200–207.
4. H. J. Kull and S. I. Anisimov, Phys. Fluids **29**, 2067 (1986).
5. H. J. Kull, Phys. Fluids B **1**, 170 (1989).
6. H. Takabe *et al*., Phys. Fluids **28**, 3676 (1985).
7. S. E. Bodner, Phys. Rev. Lett. **33**, 761 (1974).
8. D. L. Book, Plasma Phys. Control. Fusion **34**, 737 (1992).
9. R. Betti, R. L. McCrory, and C. P. Verdon, Phys. Rev. Lett. **71**, 3131 (1993).
10. J. G. Wouchuk and A. R. Piriz, Phys. Plasmas **2**, 493 (1995).
11. K. O. Mikaelian, Phys. Rev. A **46**, 6621 (1992).
12. V. V. Bychkov, S. M. Golberg, and M. A. Liberman, Phys. Plasmas **1**, 2976 (1994).
13. J. Sanz, Phys. Rev. Lett. **73**, 2700 (1994).
14. A. B. Bud'ko and M. A. Liberman, Phys. Fluids B **4**, 3499 (1992).
15. R. Betti, V. Goncharov, R. L. McCrory, E. Turano, and C. P. Verdon, Phys. Rev. E **50**, 3968 (1994).
16. R. Betti, V. N. Goncharov, R. L. McCrory, and C. P. Verdon, Phys. Plasmas **2**, 3844 (1995).
17. C. P. Verdon, R. L. McCrory, R. L. Morse, G. R. Baker, D. I. Meiron, and S. A. Orszag, Phys. Fluids **25**, 1653 (1982).
18. M. Tabak, D. H. Munro, and J. D. Lindl, Phys. Fluids B **2**, 1007 (1990).
19. J. H. Gardner, S. E. Bodner, and J. P. Dahlburg, Phys. Fluids B **3**, 1070 (1991).
20. S. V. Weber *et al*., Phys. Plasmas **1**, 3652 (1994).
21. Ya. B. Zel'dovich and Yu. P. Raizer, in *Physics of Shock Waves and High-Temperature Hydrodynamic Phenomena*, edited by W. D. Hayes and R. F. Probstein (Academic Press, New York, 1966), Vol. I, p. 152.
22. L. Spitzer, Jr. and R. Härm, Phys. Rev. **89**, 977 (1953).